Journal of Applied Mechanics Vol.10, pp.757-768 (August 2007) JSCE

Study of characteristics of inertia and viscous flow regions by means of dam break flow with finite volume.

How Tion PUAY* and Takashi HOSODA**

*PhD Student Dept. Urban Management, Kyoto Univ.
(Kyodai Katsura, Nishikyo-ku, Kyoto 615-8530)
**Member of JSCE, Professor, Dept. Urban Management, Kyoto Univ.
(Kyodai Katsura, Nishikyo-ku, Kyoto 615-8530)

In this study, the characteristics of inertia and viscous regions of shallow flow are investigated by means of dam break flow with finite volume occurring in a smooth rectangular channel. Inviscid fluid and viscous fluid, comprising of Newtonian and non-Newtonian are studied theoretically and similarity solutions describing both inertia and viscous regions are derived. Theoretical findings are verified with two numerical models: a depth averaged model and a Lagrangian grid-less model (MPS or Moving Particle Semi-Implicit).

Key Words : *inertia region, viscous region, inviscid, Newtonian and non-Newtonian fluids*

1. Introduction

Dam break flow has been well studied as it is a paradigm problem in fluid mechanics of non-linear shallow flow. It is also often used as a means to evaluate rheological properties. Hosoda *et al.*[1] treated the slump flow test of fresh concrete as a kind of dam break flow in his investigation of fresh concrete's rheological properties, while Shao & Lo[2] also used dam break flow as a means to study Newtonian and non-Newtonian fluids using numerical models.

Huppert's[3] study shows that characteristic regions exist for the propagation of front wave and the attenuation of depth of flow at the origin in dam break flow of viscous fluid. In this study, the propagation of the leading front wave and temporal variation of depth of flow at the origin are used as parameters to describe the flow characteristic. It is expected that these results will give us some useful information to evaluate properties of fluidable materials.

In this paper, an attempt is made to derive similarity solutions for the temporal variation of the front wave position L and temporal variation of the depth at the origin h_m. Meanwhile, in the derivation of flow characteristic in the viscous region, it is assumed that pressure and viscous terms are of the same order. The characteristics of viscous region for Newtonian fluid and non-Newtonian fluids are derived based on the shear stress and rate of strain relation proposed by the Power-Law model. The general form of constitutive relation of shear stress and rate of strain proposed by the Power-Law model is as follows:

$$\tau = K\left(\frac{\partial u}{\partial y}\right)^n \tag{1}$$

where $n = 1$ for Newtonian fluid, while $n < 1$ and $n > 1$ for non-Newtonian fluid.

2. Inviscid Fluid

The flow from a sudden release of mass of inviscid fluid in a dam can be adequately described by the following one-dimensional depth averaged continuity and momentum equations, as in Eq. (2) and Eq. (3).

$$\frac{\partial h}{\partial t} + \frac{\partial hV}{\partial x} = 0 \tag{2}$$

$$\frac{\partial hV}{\partial t} + \frac{\partial \widehat{\beta} hV^2}{\partial x} + gh\frac{\partial h}{\partial x} = 0 \tag{3}$$

where the parameters are described schemetically in Fig. 1 with h as the depth of flow, V as the flow velocity in x direction, ν as the kinematic viscosity, ρ as the fluid density, $\widehat{\beta}$ as the momentum coefficient and g as the gravity acceleration.

2.1 Theoretical analysis

(1) Temporal variation of depth of flow at the origin

The depth of flow h, and velocity V, are assumed to be expressible as a series of power which is applicable only in the region close to the wall. By using the Taylor's power series expansion, they can be written

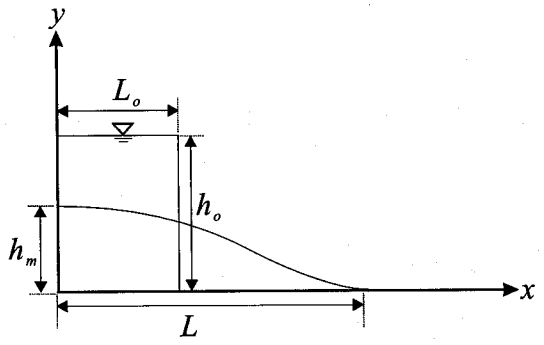

Fig. 1 Dam break flow of finite volume.

as in Eq. (4) and Eq. (5) respectively.

$$h(t) = h_m(t) + a_1(t)\left(\frac{x}{h_o}\right) + a_2(t)\left(\frac{x}{h_o}\right)^2 + a_3(t)\left(\frac{x}{h_o}\right)^3 + a_4(t)\left(\frac{x}{h_o}\right)^4 + \dots \quad (4)$$

$$V(t) = \sqrt{gh_o}\left[b_1(t)\left(\frac{x}{h_o}\right) + b_2(t)\left(\frac{x}{h_o}\right)^2 + b_3(t)\left(\frac{x}{h_o}\right)^3 + b_4(t)\left(\frac{x}{h_o}\right)^4 + \dots\right] \quad (5)$$

where h_o = representative flow depth, x = distance from the origin, $a_1(t)$, $a_2(t)$, $a_3(t)$, $a_4(t)$, $b_1(t)$, $b_2(t)$, $b_3(t)$, and $b_4(t)$ are time dependent coefficients while other parameters are defined as in Fig. 1.
By substituting the power series of h and V into the continuity and momentum equations, we can rewrite both equations again by order of power as in the following equations, Eq. (6) to Eq. (14).
Continuity Equation:
0th order

$$\frac{dh_m}{dt} + \sqrt{gh_o}\frac{h_m b_1}{h_o} = 0 \quad (6)$$

1st order

$$\frac{1}{h_o}\frac{da_1}{dt} + \frac{\sqrt{gh_o}}{{h_o}^2}\left[2h_m b_2 + 2a_1 b_1\right] = 0 \quad (7)$$

2nd order

$$\frac{1}{{h_o}^2}\frac{da_2}{dt} + \frac{\sqrt{gh_o}}{{h_o}^3}\left[3h_m b_3 + 3a_1 b_2 + 3a_2 b_1\right] = 0 \quad (8)$$

3rd order

$$\frac{1}{{h_o}^3}\frac{da_3}{dt} + \frac{\sqrt{gh_o}}{{h_o}^4}\left[4h_m b_4 + 4a_1 b_3 + 4a_2 b_2 + 4a_3 b_1\right] = 0 \quad (9)$$

4th order

$$\frac{1}{{h_o}^4}\frac{da_4}{dt} + \frac{\sqrt{gh_o}}{{h_o}^5}\left[5a_1 b_4 + 5a_2 b_3 + 5a_3 b_2 + 5a_4 b_1\right] = 0 \quad (10)$$

Momentum equation:
0th order

$$\frac{g{h_m}^2 a_1}{h_o} = 0 \quad (11)$$

1st order

$$\frac{\sqrt{gh_o}}{h_o}h_m\frac{d}{dt}(h_m b_1) + \frac{g}{h_o}\left(2{h_m}^2{b_1}^2\right) + \frac{g}{{h_o}^2}\left(2a_2{h_m}^2 + 2h_m{a_1}^2\right) = -3\nu\sqrt{gh_o}\frac{b_1}{h_o} \quad (12)$$

2nd order

$$\frac{\sqrt{gh_o}}{{h_o}^2}\left[h_m\frac{d}{dt}(h_m b_2 + a_1 b_1) + a_1\frac{d}{dt}(h_m b_1)\right] + \frac{g}{{h_o}^2}\left(6b_1 b_2{h_m}^2 + 5h_m a_1{b_2}^2\right) + \frac{g}{{h_o}^3}\left[3a_3{h_m}^2 + 4h_m a_1 a_2 + a_1\left({a_1}^2 + 2a_2 h_m\right)\right] = -3\nu\sqrt{gh_o}\frac{b_2}{{h_o}^2} \quad (13)$$

3rd order

$$\frac{\sqrt{gh_o}}{{h_o}^3}\left[h_m\frac{d}{dt}(h_m b_3 + a_1 b_2 + a_2 b_1) + \frac{a_1}{{h_o}^3}\frac{d}{dt}(h_m b_2 + a_1 b_1) + \frac{a_2}{{h_o}^3}\frac{d}{dt}(h_m b_1)\right] + \frac{g}{{h_o}^3}\left[8b_1 b_3{h_m}^2 + 6h_m a_2{b_1}^2 + 4{b_2}^2{h_m}^2 + 8b_1 b_2 h_m + 6a_1 b_1 b_2 h_m + 3a_1{b_1}^2\right] + \frac{g}{{h_o}^4}\left[4a_4{h_m}^2 + 6h_m a_1 a_3 + 2a_2\left({a_1}^2 + 2a_2 h_m\right) + a_1\left(2a_3 h_m + 2a_1 a_2\right)\right] = -3\nu\sqrt{gh_o}\frac{b_3}{{h_o}^3} \quad (14)$$

We can deduce From Eq. (11) that $a_1 = 0$. Therefore from Eq. (7), we have $b_2 = 0$. Consequently, from Eq. (13) and Eq. (9), we can further deduce $a_3 = 0$ and $b_4 = 0$. By using these results, the continuity and momentum equations can be further simplified as follows:
Continuity equation:
0th order

$$\frac{dh_m}{dt} + \sqrt{gh_o}\frac{h_m b_1}{h_o} = 0 \quad (15)$$

2nd order

$$\frac{1}{{h_o}^2}\frac{da_2}{dt} + \frac{\sqrt{gh_o}}{h_o^3}\left[3h_m b_3 + 3a_2 b_1\right] = 0 \quad (16)$$

4th order

$$\frac{1}{{h_o}^4}\frac{da_4}{dt} + \frac{\sqrt{gh_o}}{{h_o}^5}\left[5a_2 b_3 + 5a_4 b_1\right] = 0 \quad (17)$$

Momemtum equation:
1st order

$$\frac{\sqrt{gh_o}}{h_o}h_m\frac{d}{dt}(h_m b_1) + \frac{g}{h_o}\left(2{h_m}^2{b_1}^2\right) + \frac{g}{{h_o}^2}\left(2a_2{h_m}^2\right) = -3\nu\sqrt{gh_o}\frac{b_1}{h_o} \quad (18)$$

3rd order

$$\frac{\sqrt{gh_o}}{{h_o}^3}\left[h_m\frac{d}{dt}\left(h_m b_3+a_2 b_1\right)+\frac{a_2}{{h_o}^3}\frac{d}{dt}\left(h_m b_1\right)\right]$$
$$+\frac{g}{{h_o}^3}\left(8b_1 b_3 {h_m}^2+6h_m a_2 {b_1}^2\right)$$
$$+\frac{g}{{h_o}^4}\left(4a_4 {h_m}^2+4{a_2}^2 h_m\right)=-3\nu\sqrt{gh_o}\frac{b_3}{{h_o}^3} \quad (19)$$

In order to non-dimensionalize the continuity and momentum equations, a set of dimensionless parameters for t , h_m , a_2 and a_4 are introduced as in Eq. (20)

$$t'=\frac{\sqrt{gh_o}}{h_o}t,\ h'_m=\frac{h_m}{h_o},\ a'_2=\frac{a_2}{h_o},\ a'_4=\frac{a_4}{h_o} \quad (20)$$

We can therefore write the dimensionless form of continuity and momentum equations, as in Eq. (21) to Eq. (25). For inviscid fluid, $\nu=0$ is assumed.
Continuity equation:
0th order

$$\frac{dh'_m}{dt'}+h'_m b_1=0 \quad (21)$$

2nd order

$$\frac{da'_2}{dt'}+3h'_m b_3+3a'_2 b_1=0 \quad (22)$$

4th order

$$\frac{da'_4}{dt'}+5a'_2 b_3+5a'_4 b_1=0 \quad (23)$$

Momentum equation:
1st order

$${h'_m}^2\frac{db_1}{dt'}+h'_m b_1\frac{dh'_m}{dt'}+2{h'_m}^2{b_1}^2+2{a_2}'{h'_m}^2=0 \quad (24)$$

3rd order

$$2h'_m a'_2\frac{db_1}{dt'}+{h'_m}^2\frac{db_3}{dt'}+\left(a'_2 b_1+b_3 h'_m\right)\frac{dh'_m}{dt'}$$
$$+\left(h'_m b_1\right)\frac{da_2{}'}{dt'}+8b_1 b_3 {h'_m}^2+6h'_m a'_2 {b_1}^2$$
$$+\left(4a'_4 {h'_m}^2+4{a'_2}^2 h'_m\right)=0 \quad (25)$$

We can show the existence of the solution with temporal power given by,

$$h'_m=\widehat{A}{t'}^a, a'_2=\widehat{B}{t'}^b, a'_4=\widehat{C}{t'}^c, b_1=\widehat{D}{t'}^d, b_3=\widehat{E}{t'}^e \quad (26)$$

By substituting Eq. (26) into continuity and momentum equations, we can equate the coefficients of t' to obtain the following equations:

$$d=-1 \quad \text{from Eq. (21)} \quad (27)$$
$$a+e=b-1 \quad \text{from Eq.(22)} \quad (28)$$
$$b+e=c-1 \quad \text{from Eq.(23)} \quad (29)$$
$$b=-2 \quad \text{from Eq.(24)} \quad (30)$$
$$a+e=-3 \quad \text{from Eq.(25)} \quad (31)$$
$$c+a=-4 \quad \text{from Eq.(25)} \quad (32)$$

By utilizing the relationships between coefficients a, b, c, d and e in Eq. (27) to Eq. (32) and substituting them back into the dimensionless form of continuity and momentum equations in Eq. (21) to Eq. (25), we can further obtain several relationships for $\widehat{A}, \widehat{B}, \widehat{C}, \widehat{D}$ and $\widehat{E}$ as in the following equations, Eq. (33) to Eq. (37).
From Eq. (21)

$$\widehat{D}=-a \quad (33)$$

From Eq. (22)

$$\widehat{A}\widehat{E}=\frac{1}{3}\left(2+3a\right)\widehat{B} \quad (34)$$

From Eq. (23)

$$5\widehat{B}\widehat{E}=\left(6a+4\right)\widehat{C} \quad (35)$$

From Eq. (24)

$$\widehat{B}=-\frac{1}{2}a\left(a+1\right) \quad (36)$$

From Eq. (25)

$$\widehat{A}\widehat{C}=-\widehat{B}^2+\frac{1}{12}\left(9a^2+13a+6\right)\widehat{B} \quad (37)$$

By multiplying $\widehat{A}$ on both sides of Eq. (35), we obtain,

$$5\widehat{A}\widehat{E}\widehat{B}=\left(6a+4\right)\widehat{A}\widehat{C} \quad (38)$$

Therefore, by substituting Eq. (34), Eq. (36) and Eq. (37) into Eq. (38), we will obtain Eq. (39) that will lead to solving coefficient a.

$$a\left(a+1\right)\left(30a^3+56a^2+33a+6\right)=0 \quad (39)$$

The solutions for coefficient a are

$$a=-1,\ a=-\frac{2}{3},\ a=\frac{1}{10}\left(-6\pm\sqrt{6}\right),\ a\neq 0 \quad (40)$$

Therefore, the temporal variation of the depth at the origin h_m can be expressed as in Eq. (41), Eq. (42) and Eq. (43).

$$a=-1,\quad \widehat{B}=0,\quad h'_m=\widehat{A}{t'}^{-1}\rightarrow h_m\propto t^{-1} \quad (41)$$

$$a=-\frac{2}{3},\quad \widehat{B}=\frac{1}{9},\quad h'_m=\widehat{A}{t'}^{-\frac{2}{3}}\rightarrow h_m\propto t^{-\frac{2}{3}} \quad (42)$$

$$a=-\frac{1}{10}\left(-6\pm\sqrt{6}\right),\quad \widehat{B}=-\frac{1}{100}\left(-9\pm\sqrt{6}\right),$$
$$h'_m=\widehat{A}{t'}^{-\frac{1}{10}\left(-6\pm\sqrt{6}\right)}\rightarrow h_m\propto t^{-\frac{1}{10}\left(-6\pm\sqrt{6}\right)} \quad (43)$$

(2) Temporal variation of leading wave position

The temporal variation of the front wave L in an infinite volume dam break flow is solved analytically by method of characteristic (MOC)[4], and the solution is given as in Eq. (44). In the case of finite volume dam

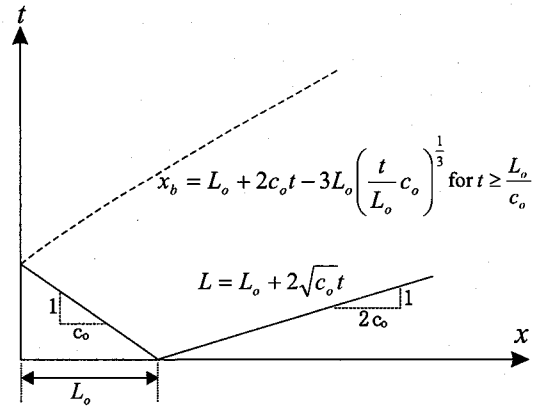

Fig. 2 Characteristic lines of dam break flow of finite volume.

break flow, the solution of the wave propagating upstream and reflected by the boundary wall is given in Eq. (45). It is obvious that this disturbance wave, x_b always trails behind the front propagation wave and therefore will not affect the flow in the region between the front wave and the disturbance wave. Since the propagation of the front wave in the dam break flow of finite volume will not be affected by the upstream boundary as shown in Fig. 2, (where c_o is the celerity), the temporal variation of the front wave position in a finite dam break flow can be expressed as in Eq. (44) as well.

$$L = L_o + 2\sqrt{gh_o}t \quad \rightarrow L \propto t \tag{44}$$

$$x_b = L_o + 2c_o t - 3L_o\left(\frac{t}{L_o}c_o\right)^{\frac{1}{3}} \tag{45}$$

2.2 Numerical Simulation Model

Moving Particle Semi-Implicit or MPS[5] is used as the numerical simulation model in this study. MPS is a grid-less particle method model. In this model, the interaction of a particle with its neighbors is taken into account through the introduction of a weight function with radius of interaction r_e. Meanwhile the number of particle per unit volume can be approximated in this model by introducing particle number density. The weight function and particle density number are defined as in Eq. (46) and Eq. (47)
Weight function:

$$w(r) = \begin{cases} \frac{r_e}{r} - 1 & \text{for } (0 \leq r < r_e) \\ 0 & \text{for } (r_e \leq) \end{cases} \tag{46}$$

Particle density number:

$$\langle n \rangle_i = \sum_{j \neq i} w(|\widetilde{r_j} - \widetilde{r_i}|) \tag{47}$$

The governing equations in this model are the conservation of mass and momentum equations as in Eq. (48) and Eq. (49).

$$\frac{D\rho}{Dt} = 0 \tag{48}$$

$$\frac{D\widetilde{u}}{Dt} = -\frac{1}{\rho}\nabla P + \nu\nabla^2\widetilde{u} + \widetilde{g} \tag{49}$$

where ρ = fluid density, P = pressure, ν = kinematic viscosity, $\widetilde{u}$ = velocity vector and $\widetilde{g}$ = gravity acceleration vector. The differential and divergence terms, as well as the Laplacian operator in the momentum equation are modified to accommodate the interaction of particles[5] as given in Eq. (50) and Eq. (51). In the case of inviscid fluid, the viscous term $\nu\nabla^2\widetilde{u}$ can be omitted since $\nu = 0$ for inviscid fluid.
Divergence model

$$\langle \nabla \cdot u \rangle = \frac{d}{n^o}\sum_{j \neq i}\frac{(\widetilde{u_j} - \widetilde{u_i}) \cdot (\widetilde{r_j} - \widetilde{r_i})}{|\widetilde{r_j} - \widetilde{r_i}|} \tag{50}$$

Laplacian model

$$\langle \nabla^2\phi \rangle = \sum_{j \neq i}(\phi_j - \phi j)\, w\left(\widetilde{\phi_j} - \widetilde{\phi j}\right)$$

$$\text{where} \quad \lambda = \frac{\int_{volume} w(r) r^2\, dv}{\int_{volume} w(r)\, dv} \tag{51}$$

MPS is chosen due to its simplicity grid-less pre-simulation set up and the ability to define complicated free-surface flow[6]. The second model that is used for the numerical analysis is a depth averaged model with Harten's TVD (Total Variation Diminishing) scheme being used in the discretization of the governing equations.

2.3 Numerical Simulation Results

The simulation of dam break flow is carried out for inviscid fluid in an infinitely long, dry, prismatic rectangular channel. The initial condition of the dam reservoir is set to a finite size of 0.5m in depth and 0.5m in length in both MPS and depth averaged models. The initial conditions of the simulation are shown in Table 1. The temporal variation of depth at the origin h_m and the front wave position L for both models are plotted in Fig. 4, while the dam break flow profiles for both models are shown in Fig. 3.

The numerical results shown in Fig. 4 show that the temporal variation of L agrees satisfactorily with the analytical results ($L \propto t$). However, in the case of temporal variation of depth at the origin h_m, the analytical analysis yields two different results as in Eq. (41) and Eq. (42). The numerical analysis results satisfy the first relation of $h_m \propto t^{-1}$ when $a = -1$; therefore allowing us to write the temporal variation of h_m as in Eq. (53)

$$a = -1,$$
$$\therefore \widehat{B} = \widehat{C} = \widehat{D} = \widehat{E} = 0 \tag{52}$$

Table 1 Initial conditions of simulation for inviscid fluid.

Model	$h_o(m)$	$L_o(m)$	$\nu(m^2s^{-1})$
MPS	0.5	0.5	0.0
Depth Averaged Model	0.5	0.5	0.0

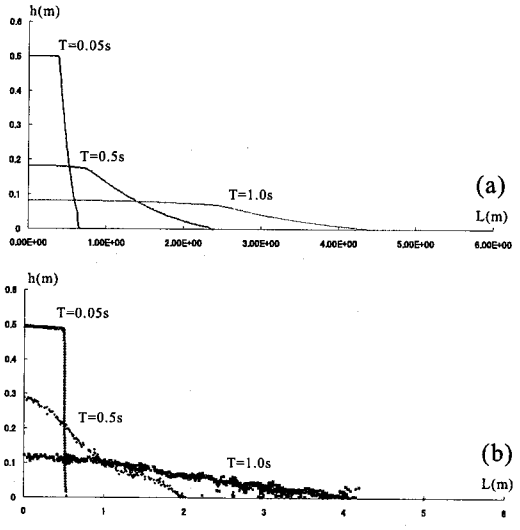

Fig. 3 Profile of dam break flow of inviscid fluid using (a) depth averaged model, (b) MPS model, with initial dam size of $h_o = 0.5m$ and $L_o = 0.5m$.

$$h(t) = \widehat{A}t'^{-1}h_o \tag{53}$$

Eq. (53) implies a flat free-surface profile near the origin, which is observed in the numerical simulation. As for the second and third relations derived for h_m, as in Eq. (54) and Eq. (56), they however imply concave free surface profile near the origin, as shown in Eq. (55) and Eq.(57) which were not observed in the numerical simulation.

$$h_m \propto t^{-\frac{2}{3}}, \text{ as } a = -\frac{2}{3} \tag{54}$$

$$\widehat{B} = \frac{1}{9},\ \widehat{C} \neq \widehat{D} \neq \widehat{E} \neq 0,$$

$$h(t) = \widehat{A}t'^{-\frac{2}{3}}h_o + \frac{1}{9}\frac{x^2}{h_o}t'^{-2} + .. \tag{55}$$

$$h_m \propto t^{-\frac{1}{10}\left(-6\pm\sqrt{6}\right)}, \text{ as } a = -\frac{1}{10}\left(-6 \pm \sqrt{6}\right) \tag{56}$$

$$\widehat{B} = -\frac{1}{100}\left(-9 \pm \sqrt{6}\right),$$

$$\widehat{C} \neq \widehat{D} \neq \widehat{E} \neq 0,$$

$$h(t) = \widehat{A}t'^{-\frac{2}{3}}h_o + \frac{1}{100}\left(9 \mp \sqrt{6}\right)\frac{x^2}{h_o}t'^{-2} + .. \tag{57}$$

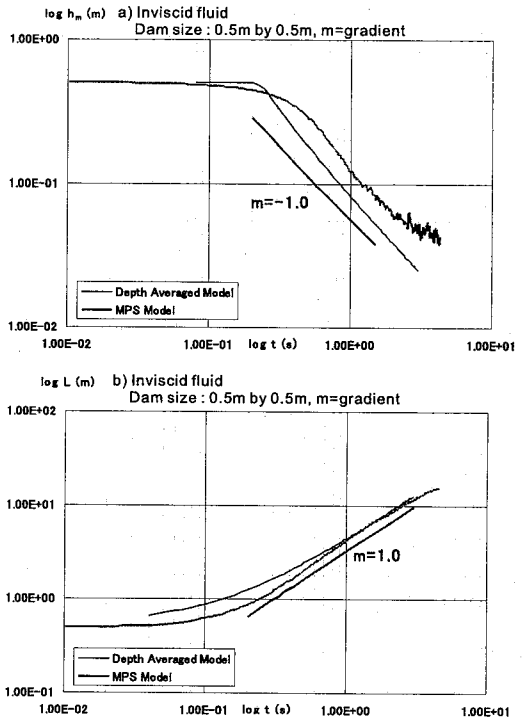

Fig. 4 (a) temporal variation of depth at the origin h_m, for inviscid fluid, (b) temporal variation of front wave propagation L, for inviscid fluid.

3. Newtonian Fluid

3.1 Theoretical Analysis

The governing equations for viscous fluid can be written as in Eq. (58).

$$\frac{D\widetilde{U}}{Dt} = -\frac{\nabla P}{\rho} + \widetilde{g} + \frac{1}{\rho}\nabla \cdot \tau \tag{58}$$

In the x direction, for two dimensional case, the equation of motion can be written as follows:

$$\frac{\partial u}{\partial t} + u\frac{\partial u}{\partial t} + v\frac{\partial u}{\partial t} = -\frac{1}{\rho}\frac{\partial P}{\partial x} + g_x + \frac{1}{\rho}\left(\frac{\partial \tau_{yx}}{\partial y} + \frac{\partial \tau_{xx}}{\partial x}\right) \tag{59}$$

By neglecting the inertia term through the assumption that the flow is slow and inertia term is small compared to viscous and pressure term, we can reduce Eq. (59) to the following form:

$$\frac{\partial P}{\partial x} = \frac{1}{\rho}\frac{\partial \tau_{yx}}{\partial y} \quad \text{as} \quad g_x = 0 \quad \text{and}$$

$$\frac{\partial \tau_{xx}}{\partial x} = 0 \quad \text{as} \quad \frac{\partial u}{\partial x} \ll \frac{\partial u}{\partial y} \tag{60}$$

Assuming static pressure distribution, $P = \rho g h$, and by integrating over the depth of flow, h,

$$\tau_{yx} = \int \frac{\partial P}{\partial x}\, dy$$

$$\tau_{yx} = -\rho g \frac{dh}{dx}(y - h) \tag{61}$$

By Power-Law model defining the general shear stress and rate of strain relation, with K= viscosity coefficient or consistency,

$$\tau = K\left(\frac{\partial u}{\partial y}\right)^n \tag{62}$$

$$K\left(\frac{\partial u}{\partial y}\right)^n = \rho g \frac{dh}{dx}(h-y) \tag{63}$$

$$\left(\frac{\partial u}{\partial y}\right)^n = R(h-y) \quad \text{with} \quad R = \frac{\rho g}{K}\left(\frac{\triangle h}{L}\right) \tag{64}$$

$$\frac{\partial u}{\partial y} = R^{\frac{1}{n}}(h-y)^{\frac{1}{n}} \tag{65}$$

$$u = \frac{n}{n+1}R^{\frac{1}{n}}\left[(h)^{\frac{1}{n}+1} - (h-y)^{\frac{1}{n}+1}\right] \tag{66}$$

From velocity distribution derived in Eq. (66), we can therefore also derive the average velocity in x direction, $\overline{U}$.

$$\begin{aligned}\overline{U}h &= \int_0^h u\,dy \\ &= \frac{n}{2n+1}R^{\frac{1}{n}}h^{2+\frac{1}{n}} \\ \overline{U} &= \frac{n}{2n+1}R^{\frac{1}{n}}h^{1+\frac{1}{n}}\end{aligned} \tag{67}$$

This velocity distribution satisfies non-slip condition at the bottom boundary and vanishing shear stress at the free surface. The velocity distribution derived in Eq. (67) also agrees with the velocity distribution of viscous fluid derived by Ng & Mei[7] and Huang & Garcia[8], and is given in the following equation:

$$u = \overline{U}\frac{2n+1}{n+1}\left[1 - \left(1 - \frac{y}{h}\right)^{\frac{1}{n}+1}\right] \tag{68}$$

with $\overline{U}$ as the average velocity as in Eq. (67).

The one dimensional depth averaged continuity and momentum equations in its general form is shown as in Eq. (69) and Eq. (70), with $\overline{U}$ as the depth averaged velocity,

$$\frac{\partial h}{\partial t} + \frac{\partial}{\partial x}\left(h\overline{U}\right) = 0 \tag{69}$$

$$\frac{\partial h\overline{U}}{dt} + \frac{\partial}{\partial x}\left(\widehat{\beta}h\overline{U}^2\right) + gh\frac{\partial h}{\partial x} = -\frac{\tau_b}{\rho} \tag{70}$$

By referring to Eq. (61), we can write the bottom shear stress, τ_b as follows:

$$\tau_b = \rho g \frac{\triangle h}{L}h \tag{71}$$

By rearranging the equation Eq. (67) for average velocity, we can relate bottom shear stress τ_b with average velocity, $\overline{U}$ as in the following equations:

Averaged velocity,

$$\begin{aligned}\overline{U} &= \frac{n}{2n+1}R^{\frac{1}{n}}h^{1+\frac{1}{n}} \\ &= \frac{n}{2n+1}\left[\frac{\rho g}{K}\cdot\frac{\triangle h}{L}\cdot h\right]^{\frac{1}{n}}h \\ \overline{U} &= \frac{n}{2n+1}\left(\frac{1}{K}\right)^{\frac{1}{n}}(\tau_b)^{\frac{1}{n}}h\end{aligned} \tag{72}$$

Therefore,

$$\tau_b = K\left(\frac{2n+1}{n}\right)^n\left(\frac{\overline{U}}{h}\right)^n \tag{73}$$

The relation in Eq. (73) also agrees with the derivation made by Ng & Mei[7], as given in Eq. (74)

$$\begin{aligned}&\tau_b = c_n\mu_n\left(\frac{\overline{U}}{h}\right)^n \text{ where } \mu_n = \text{viscosity coefficient,} \\ &c_n = \left(\frac{2n+1}{n}\right)\end{aligned} \tag{74}$$

By using the relation of bottom shear stress τ_b and the average velocity $\overline{U}$, we can therefore rewrite the one dimensional depth averaged equation of motion for general viscous fluid as follows:
Continuity equation

$$\frac{\partial h}{\partial t} + \frac{\partial}{\partial x}(hV) = 0 \tag{75}$$

Momentum equation

$$\begin{aligned}&\frac{\partial hV}{\partial t} + \frac{\partial}{\partial x}\left(\widehat{\beta}hV^2\right) + gh\frac{\partial h}{\partial x} = -\frac{\tau_b}{\rho} \\ &= -\frac{K}{\rho}\left(\frac{2n+1}{n}\right)\left(\frac{V}{h}\right)^n \\ &= -3\nu\left(\frac{V}{h}\right) \text{ for Newtonian fluid}\end{aligned} \tag{76}$$

In the case of viscous Newtonian fluid, n=1 and viscosity coefficient, K is normally written as μ. Therefore, the last term on the right hand side of Eq. (76) can be written as $-3\nu\left(\frac{V}{h}\right)$ for viscous Newtonian fluid.

Similarity functions $p\left(\frac{x}{L}\right)$ and $q\left(\frac{x}{L}\right)$ are being introduced for the depth of flow h and velocity of flow V respectively. Therefore, the depth of flow h and its respective velocity V at x can be expressed as in Eq. (77) and Eq. (78), where L is the front wave tip position of the flow measured from the origin, as shown in Fig. 1.

$$h = h_m(t)\,p\left(\frac{x}{L(t)}\right) \tag{77}$$

$$V = V_m(t)\,q\left(\frac{x}{L(t)}\right) \tag{78}$$

As the front tip of the flow L is a function of time, parameter ξ is introduced, where ξ is defined as in the following equation:

$$\xi = \frac{x}{L(t)} \tag{79}$$

The boundary condition for the similarity functions, $p(\xi)$ and $q(\xi)$ can therefore be written as follows:

$$p(0)=1,\ p(1)=0,\ \text{and}\ q(0)=0 \tag{80}$$

Meanwhile, total volume of the flow can be expressed as the integration of the flow depth along the flow, as in the following equation:

$$\begin{aligned}\text{Volume of flow} &= \int_0^L h\,dx \\ &= h_m \int_0^L p\left(\frac{x}{L}\right) dx \\ &= h_m L \int_0^1 p(\xi)\,d\xi \end{aligned} \tag{81}$$

By substituting the depth of flow h and velocity of flow V, expressed in their similarity function $p(\xi)$ and $q(\xi)$, we can rewrite the governing equations as follows:
Continuity equation

$$\frac{\partial}{\partial t}\left[h_m(t)\,p(\xi)\right]+\frac{\partial}{\partial x}\left[h_m(t)\,p(\xi)\,V_m(t)\,q(\xi)\right]=0 \tag{82}$$

Rearangging Eq. (82)

$$\begin{aligned}&p(\xi)\frac{\partial h_m}{\partial t}-\frac{h_m\xi}{L}\frac{\partial p(\xi)}{\partial \xi}\frac{\partial L}{\partial t}+\frac{h_m V_m}{L}p(\xi)\frac{\partial q(\xi)}{\partial \xi}\\ &+\frac{h_m V_m}{L}q(\xi)\frac{\partial p(\xi)}{\partial \xi}=0\end{aligned} \tag{83}$$

Momentum equation

$$\begin{aligned}&\frac{\partial}{\partial t}\left[h_m p(\xi)\,V_m q(\xi)\right]+\frac{\partial}{\partial x}\left[\widehat{\beta}h_m p(\xi)\,{V_m}^2 q^2(\xi)\right]\\ &+g{h_m}^2\frac{p(\xi)}{L}\frac{\partial p(\xi)}{\partial \xi}=-3\nu\frac{V_m q(\xi)}{h_m p(\xi)}\end{aligned} \tag{84}$$

Rearranging Eq. (84)

$$\begin{aligned}&h_m p(\xi)\left[q(\xi)\frac{\partial V_m}{\partial t}-V_m\frac{\xi}{L}\frac{\partial q}{\partial \xi}\frac{\partial \xi}{\partial t}\right]\\ &+V_m q(\xi)\left[p(\xi)\frac{\partial h_m}{\partial t}-h_m\frac{\xi}{L}\frac{\partial p}{\partial \xi}\frac{\partial \xi}{\partial t}\right]\\ &+\widehat{\beta}\frac{{V_m}^2 h_m}{L}q^2(\xi)\frac{\partial p(\xi)}{\partial \xi}+2\widehat{\beta}\frac{{V_m}^2 h_m}{L}p(\xi)\,q(\xi)\frac{\partial q(\xi)}{\partial \xi}\\ &+g\frac{{h_m}^2}{L}p(\xi)\frac{\partial p(\xi)}{\partial \xi}=-3\nu\frac{V_m q(\xi)}{h_m p(\xi)}\end{aligned} \tag{85}$$

By assuming similarity solutions exist for h_m, V_m and L, we can introduce the following equations:

$$h_m=\alpha h_o\left(\sqrt{\frac{g}{h_o}}t\right)^a \tag{86}$$

$$V_m=\beta\sqrt{gh_o}\left(\sqrt{\frac{g}{h_o}}t\right)^b \tag{87}$$

$$L=\gamma L_o\left(\sqrt{\frac{g}{h_o}}t\right)^c \tag{88}$$

where h_o is the characteristic depth and L_o is the characteristic length. The dimensionless form of t is defined as follows:

$$t'=\sqrt{\frac{g}{h_o}}t \tag{89}$$

Therefore, by substituting the similarity form of h_m, V_m and L, as well as the dimensionless form of t, we can further write the governing equations as follows:
Continuity Equation

$$\begin{aligned}&\alpha h_o a {t'}^{a-1}\sqrt{\frac{g}{h_o}}p(\xi)-\alpha h_o a c {t'}^{a-1}\xi\sqrt{\frac{g}{h_o}}\frac{\partial p(\xi)}{\partial \xi}\\ &+\frac{\alpha\beta}{\gamma L_o}h_o\sqrt{gh_o}\,q(\xi)\frac{\partial p(\xi)}{\partial \xi}{t'}^{a+b-c}\\ &+\frac{\alpha\beta}{\gamma L_o}h_o\sqrt{gh_o}\,p(\xi)\frac{\partial q(\xi)}{\partial \xi}{t'}^{a+b-c}=0\end{aligned} \tag{90}$$

Momentum Equation

$$\begin{aligned}&\alpha\beta b g h_o p(\xi)\,q(\xi)\,{t'}^{a+b-1}-\alpha\beta c g h_o \xi p(\xi)\frac{\partial q(\xi)}{\partial \xi}\\ &{t'}^{a+b-1}+\alpha\beta a g h_o p(\xi)\,q(\xi)\,{t'}^{a+b-1}-\alpha\beta c g h_o \xi q(\xi)\\ &\frac{\partial p(\xi)}{\partial \xi}{t'}^{a+b-1}+\widehat{\beta}\frac{\alpha\beta^2}{\gamma}\frac{g{h_o}^2}{L_o}q^2(\xi)\frac{\partial p(\xi)}{\partial \xi}{t'}^{a+2b-c}\\ &+2\widehat{\beta}\frac{\alpha\beta^2}{\gamma}\frac{g{h_o}^2}{L_o}p(\xi)\,q(\xi)\frac{\partial q(\xi)}{\partial \xi}{t'}^{a+2b-c}\\ &+\frac{\alpha^2}{\gamma}\frac{g{h_o}^2}{L_o}p(\xi)\frac{\partial p(\xi)}{\partial \xi}{t'}^{2a-c}=-3\nu\frac{\beta}{\alpha}\sqrt{\frac{g}{h_o}}\frac{q(\xi)}{p(\xi)}{t'}^{b-a}\end{aligned} \tag{91}$$

To satisfy dimensional homogeneity, we therefore equate the power of t' in Eq. (90),
From continuity equation

$$a-1=a+b-c\quad\rightarrow\quad b-c=-1 \tag{92}$$

From volume of flow, as defined in Eq. (81)

$$\begin{aligned}V&=h_m L\int_0^1 p(\xi)\,d\xi\\ &=\alpha h_o\left(\sqrt{\frac{g}{h_o}}t\right)^a\gamma L_o\left(\sqrt{\frac{g}{h_o}}t\right)^c\int_0^1 p(\xi)\,d\xi\end{aligned} \tag{93}$$

As the volume of flow is assumed to be constant during the whole dam break duration;

$$a+c=0 \tag{94}$$

In the case of flow of viscous fluid, it is assumed that in the viscous region, the flow propagates under the dynamic equilibrium of pressure and viscosity. Therefore, by equating the power of t' of the pressure term and viscous term in the momentum equation, Eq. (90), we can write the following relations between the coefficients a, b and c.

$$2a+c=b-a \tag{95}$$

Table 2 Initial conditions of simulations for viscous fluid.

Model	$h_o(m)$	$L_o(m)$	$\nu(m^2s^{-1})$
MPS	0.5	0.5	0.000001
MPS	0.5	0.5	0.00005
MPS	0.5	0.5	0.0005
MPS	0.5	0.5	0.001

By solving Eq. (92), Eq. (94) and Eq. (95) for coefficients a, b and c, we have,

$$a = -\frac{1}{5}, \quad b = -\frac{4}{5} \quad c = \frac{1}{5} \tag{96}$$

Thus, we can write the following relations for depth of flow at the origin h_m and the front wave position L as follows:

$$h_m = \alpha h_o \left(\sqrt{\frac{g}{h_o}}t\right)^a \quad \rightarrow \quad h_m \propto t^{-\frac{1}{5}} \tag{97}$$

$$L = \gamma L_o \left(\sqrt{\frac{g}{h_o}}t\right)^c \quad \rightarrow \quad L \propto t^{\frac{1}{5}} \tag{98}$$

3.2 Numerical Simulation Results

The simulation of dam break flow for viscous fluid is carried out in the same condition as in the case of inviscid fluid, except that non-slip condition is created for the wall and floor of the channel. Table 2. shows the initial condition and kinematic viscosity, ν used in the numerical simulation. The simulation results of viscous Newtonian fluid are shown in Fig. 5 and Fig. 6. The simulation results show good agreement with the results obtained from the theoretical analysis. Distinct regions can be observed for the temporal variation of depth at the origin h_m and front wave position of the flow L. These region define the inertia and viscous regions of the flow. In the viscous region, the depth at the origin and the front wave position are proportional to time to the power of $-\frac{1}{5}$ and $\frac{1}{5}$ respectively. Huppert[3] also observes the same results for the propagation of front wave L and depth of flow at the origin h_m in the viscous region for the case of Newtonian fluid.

The initial region which defines a short moment immediately after the release of the mass of fluid in the dam shown in the numerical results could not be verified analytically. This is because there exists no similarity solution in the initial region shortly after the motion is initiated, and therefore the analytical results only yield characteristics defining regions where similarity assumptions are valid.

4. Non-Newtonian Fluid

4.1 Theoretical Analysis

The one dimensional depth averaged continuity and momentum equations for general viscous fluid obeying the the Power Law model are derived as in Eq. (75) and Eq. (76). For simplicity, non-Newtonian fluid is studied in the case of $n > 1$ for shear thickening fluid and $n < 1$ for shear thinning fluid. The same method of introducing similarity functions of p and q, and assuming power law relating to time for h_m, V_m and L in the investigation of viscous Newtonian fluid is used here as well. Therefore, the continuity and momentum equations for non-Newtonian fluid can be written again as follows:
Continuity Equation:

$$\begin{aligned}
&\alpha h_o a t'^{a-1}\sqrt{\frac{g}{h_o}}p(\xi) - \alpha h_o a c t'^{a-1}\xi\sqrt{\frac{g}{h_o}}\frac{dp(\xi)}{d\xi} \\
&+\frac{\alpha\beta}{\gamma L_o}h_o\sqrt{gh_o}\,q(\xi)\frac{dp(\xi)}{d\xi}t'^{a+b-c} \\
&+\frac{\alpha\beta}{\gamma L_o}h_o\sqrt{gh_o}\,p(\xi)\frac{dq(\xi)}{d\xi}t'^{a+b-c} = 0
\end{aligned} \tag{99}$$

Momentum Equation:

$$\begin{aligned}
&\alpha\beta b g h_o p(\xi)\,q(\xi)\,t'^{a+b-1} \\
&-\alpha\beta c g h_o \xi p(\xi)\frac{dq(\xi)}{d\xi}t'^{a+b-1} \\
&+\alpha\beta a g h_o p(\xi)\,q(\xi)\,t'^{a+b-1} \\
&-\alpha\beta c g h_o \xi q(\xi)\frac{dp(\xi)}{d\xi}t'^{a+b-1} \\
&+\widehat{\beta}\frac{\alpha\beta^2}{\gamma}\frac{g{h_o}^2}{L_o}q^2(\xi)\frac{dp(\xi)}{d\xi}t'^{a+2b-c} \\
&+2\widehat{\beta}\frac{\alpha\beta^2}{\gamma}\frac{g{h_o}^2}{L_o}p(\xi)\,q(\xi)\frac{dq(\xi)}{d\xi}t'^{a+2b-c} \\
&+\frac{\alpha^2}{\gamma}\frac{g{h_o}^2}{L_o}p(\xi)\frac{dp(\xi)}{d\xi}t'^{2a-c} \\
&=\frac{K}{\rho}\left(\frac{2n+1}{n}\right)^n\left(\frac{\beta}{\alpha}\sqrt{\frac{g}{h_o}}\frac{p(\xi)}{p(\xi)}t'^{b-a}\right)^n
\end{aligned} \tag{100}$$

By equating the power of t' in the continuity equation, as in Eq. (99), the following relations of coefficients a b and c are obtained,
From continuity equation

$$a - 1 = a + b - c \quad \rightarrow \quad b - c = -1 \tag{101}$$

For constant volume of flow

$$\begin{aligned}
V &= h_m L\int_0^1 p(\xi)\,d\xi \\
&= \alpha h_o\left(\sqrt{\frac{g}{h_o}}t\right)^a \gamma L_o\left(\sqrt{\frac{g}{h_o}}t\right)^c\int_0^1 p(\xi)\,d\xi
\end{aligned} \tag{102}$$

Therefore

$$a + c = 0 \tag{103}$$

Similar to the procedure in the investigation of viscous Newtonian fluid, the dynamic equilibrium between viscous term and pressure term is assumed to

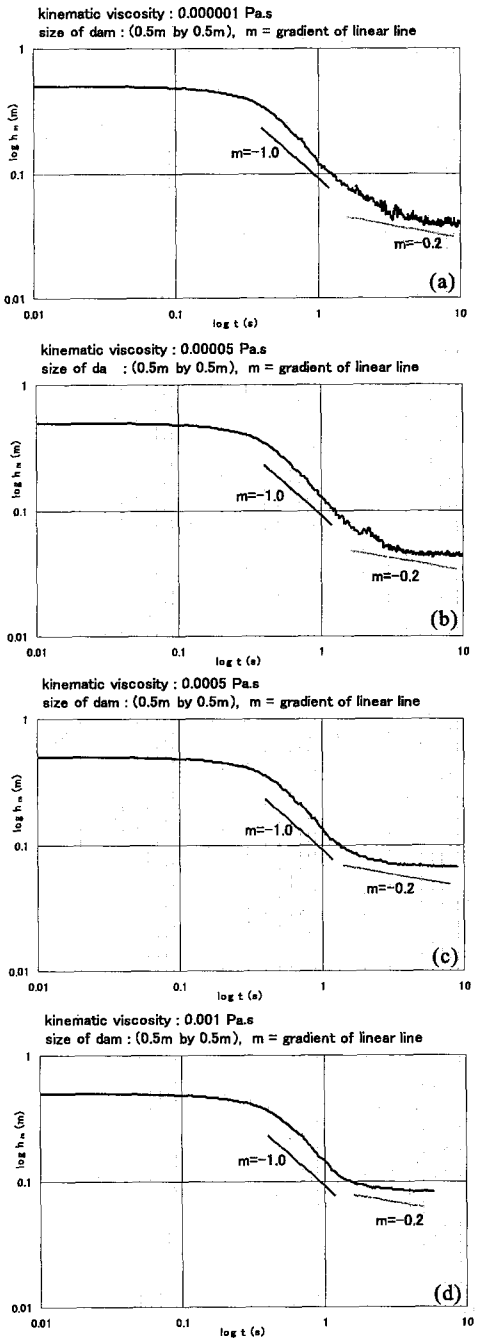

Fig. 5 Temporal variation of depth at the origin, h_m for a) $\nu = 0.000001\,m^2s^{-1}$, b) $\nu = 0.00005\,m^2s^{-1}$, c) $\nu = 0.0005\,m^2s^{-1}$, d) $\nu = 0.001\,m^2s^{-1}$.

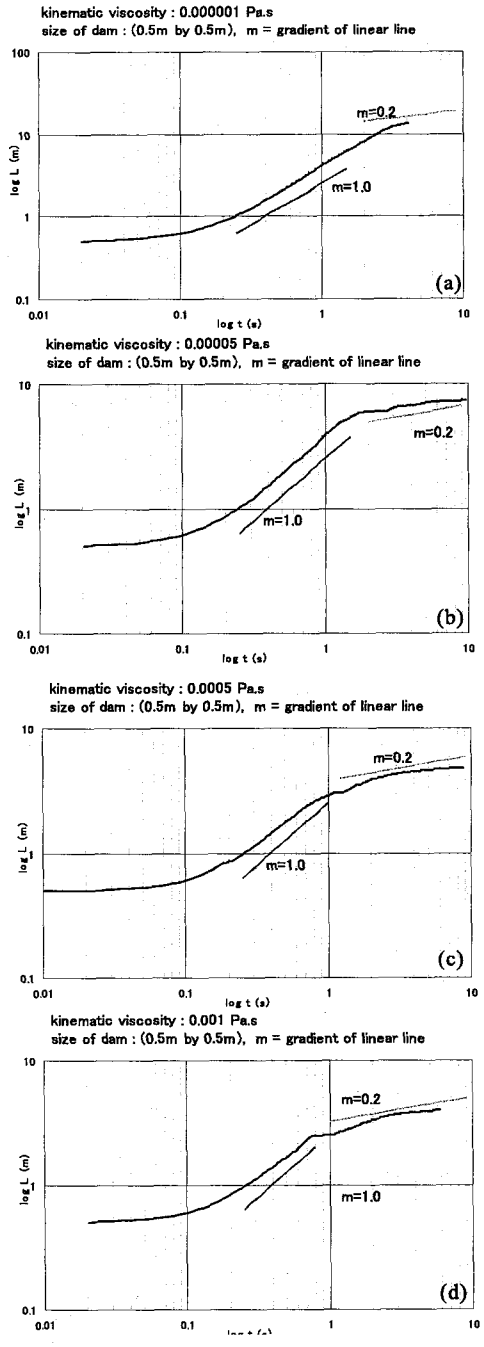

Fig. 6 Temporal variation of front wave propagation, L for a) $\nu = 0.000001\,m^2s^{-1}$, b) $\nu = 0.00005\,m^2s^{-1}$, c) $\nu = 0.0005\,m^2s^{-1}$, d) $\nu = 0.001\,m^2s^{-1}$.

exist in the viscous region of the flow.
Therefore, by equating the viscous term and pressure term in the equation of motion, we have,

$$2a - c = n(b - a) \tag{104}$$

By solving Eq. (101), Eq. (103) and Eq. (104), solutions for coefficients a and c are obtained,

$$a = -\frac{n}{3+2n} \tag{105}$$

$$c = \frac{n}{3+2n} \tag{106}$$

Thus, the front wave position L and depth of flow at the origin h_m can be written as:

$$h_m = \alpha h_o \left(\sqrt{\frac{g}{h_o}}t\right)^a \quad \rightarrow \quad h_m \propto t^{-\frac{n}{3+2n}} \tag{107}$$

$$L = \gamma L_o \left(\sqrt{\frac{g}{h_o}}t\right)^c \quad \rightarrow \quad L \propto t^{\frac{n}{3+2n}} \tag{108}$$

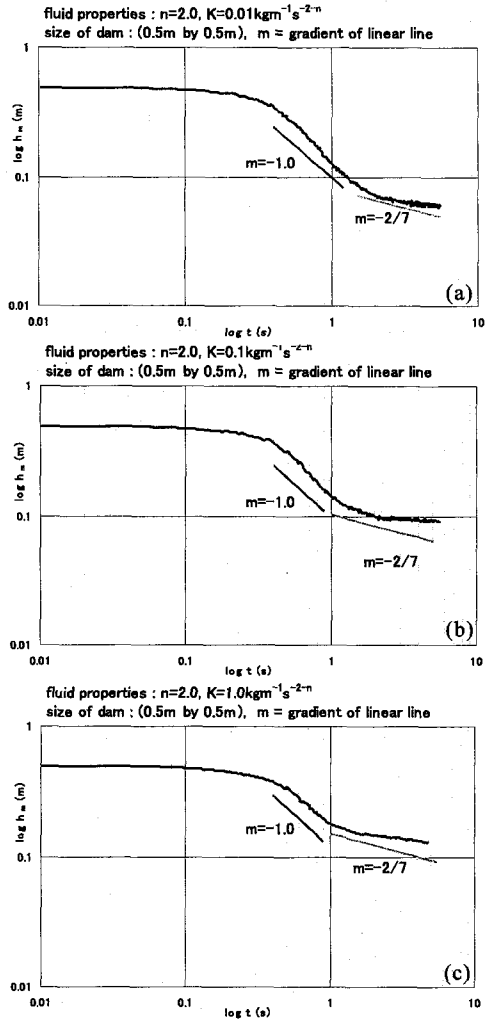

Fig. 7 Temporal variation of depth at origin, h_m for $n = 2.0$ with (a) $K = 0.01\,kgm^{-1}s^{-4}$, (b) $K = 0.1\,kgm^{-1}s^{-4}$, (c) $K = 1.0\,kgm^{-1}s^{-4}$.

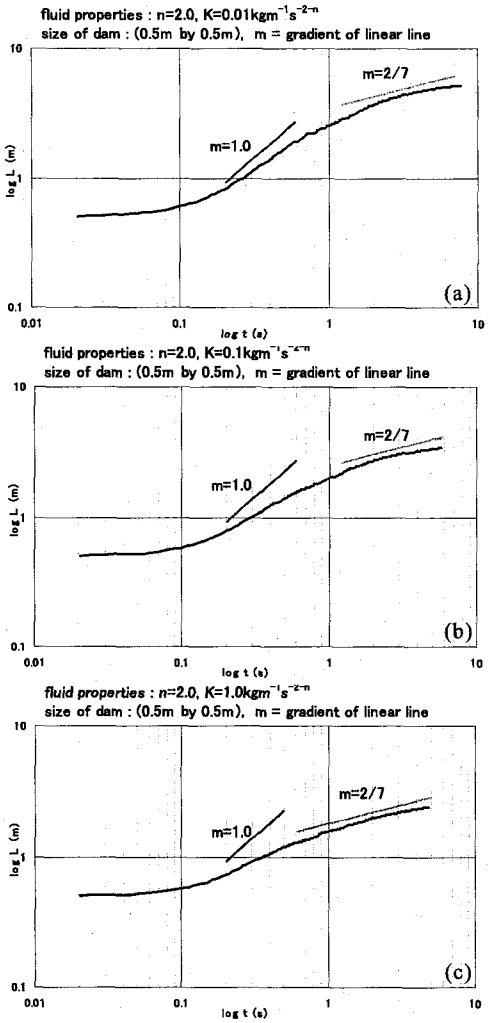

Fig. 8 Temporal variation of front wave propagation, L for $n = 2.0$ with (a) $K = 0.01\,kgm^{-1}s^{-4}$, (b) $K = 0.1\,kgm^{-1}s^{-4}$, (c) $K = 1.0\,kgm^{-1}s^{-4}$.

The results in Eq. (107) and Eq. (108) can be used for any fluid obeying the constitutive law in the power law model. For Newtonian fluid (n=1), therefore the temporal propagation of leading front, L and temporal variation of depth at the origin, h_m for Newtonian fluid are as follows:

$$h_m \propto t^{-\frac{1}{5}} \tag{109}$$

$$L \propto t^{\frac{1}{5}} \tag{110}$$

which agree with the theoretical derivation made in Section 3.1.

4.2 Numerical Simulation Results

Numerical simulation of non-Newtonian fluid is carried out using MPS model as well. But, the viscous term in the governing equation of MPS model has to be modified to take into account the constitutive law of non-Newtonian fluid. The viscous term is modified as follows:

$$\begin{aligned}\frac{1}{\rho}\frac{\partial \tau_{ij}}{\partial x_i} &= \frac{1}{\rho}\frac{\partial}{\partial x_j}\left[K\left(\frac{\partial u_i}{\partial x_j}\right)^n\right] \\ &= \frac{1}{\rho}\frac{\partial}{\partial x_j}Kn\left(\frac{\partial u_i}{\partial x_j}\right)^{n-1}\left(\frac{\partial^2 u_i}{\partial {x_j}^2}\right) \\ &= \frac{1}{\rho}Kn\left(\nabla u\right)^{n-1}\left(\nabla^2 u\right)\end{aligned} \tag{111}$$

where ∇u and $\nabla^2 u$ are the gradient and Laplacian form used in MPS model. The initial conditions of dam break flow simulation for non-Newtonian fluid are shown in Table 3, with n=2.0 assumed for shear thickening fluid and n=0.5 for shear thinning fluid. The results of simulation of non-Newtonian fluid are shown in Fig. 7, Fig. 8, Fig. 9 and Fig. 10. In both cases of shear thickening ($n = 2.0$) and shear thinning ($n = 0.5$) fluids, distinct inertia and viscous regions are observed. Both shear thickening and shear

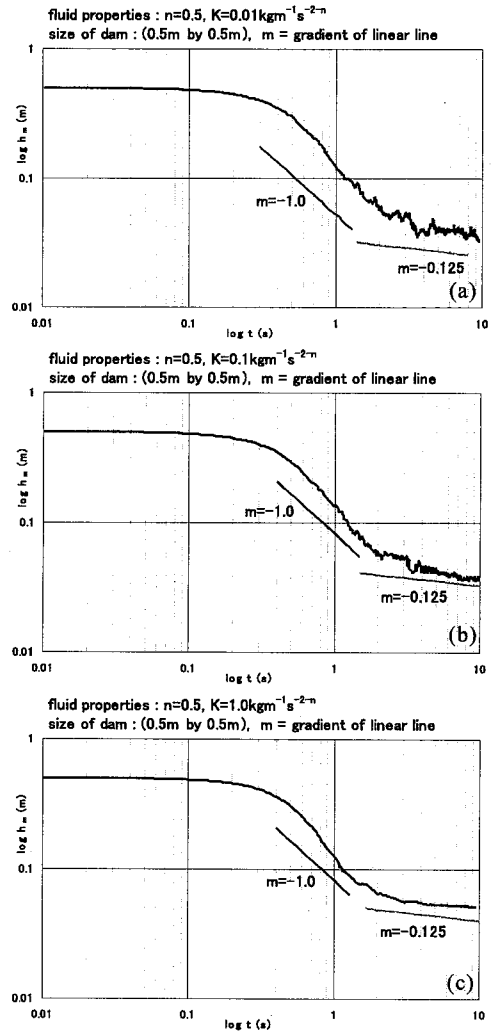

Fig. 9 Temporal variation of depth at origin, h_m for $n = 0.5$ with (a) $K = 0.01\,kgm^{-1}s^{-\frac{5}{2}}$, (b) $K = 0.1\,kgm^{-1}s^{-\frac{5}{2}}$, (c) $K = 1.0\,kgm^{-1}s^{-\frac{5}{2}}$.

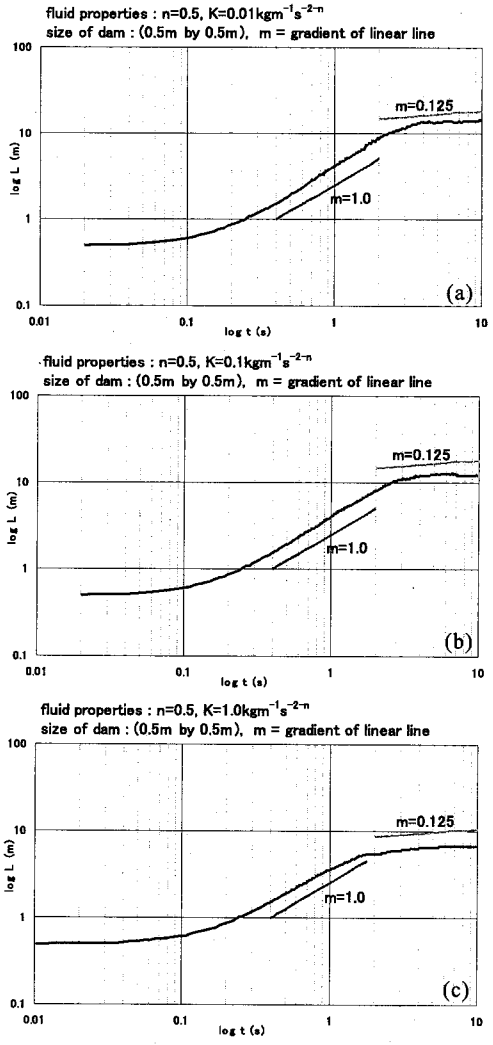

Fig. 10 Temporal variation of front wave propagation, L for $n = 0.5$ with (a) $K = 0.01\,kgm^{-1}s^{-\frac{5}{2}}$, (b) $K = 0.1\,kgm^{-1}s^{-\frac{5}{2}}$, (c) $K = 1.0\,kgm^{-1}s^{-\frac{5}{2}}$.

thinning fluids also show good agreement with the theoretical analysis in the viscous region, where in the case of shear thickening fluid ($n = 2.0$) and shear thinning fluid ($n = 0.5$), the depth at the origin h_m and propagation of front wave position is related to time as follows:
For n=2.0

$$h_m \propto t^{-\frac{2}{7}}$$
$$L \propto t^{\frac{2}{7}} \qquad (112)$$

For n=0.5

$$h_m \propto t^{-\frac{1}{8}}$$
$$L \propto t^{\frac{1}{8}} \qquad (113)$$

The viscous region becomes more dominant over the inertia region as consistency K is being increased for both shear thickening and shear thinning fluids.

Table 3 Initial conditions of simulation for non-Newtonian fluids.

Non-Newtonian Fluids	$h_o(m)$	$L_o(m)$	K
Shear thickening			
$n = 2.0$	0.5	0.5	0.01
$n = 2.0$	0.5	0.5	0.1
$n = 2.0$	0.5	0.5	1.0
Shear thinning			
$n = 0.50$	0.5	0.5	0.01
$n = 0.50$	0.5	0.5	0.1
$n = 0.50$	0.5	0.5	1.0

5. Conclusion

In this study, the motion of fluid is modeled by the sudden release of mass of fluid in a dam, which is also

known as the classical dam break flow problem. In the absence of viscosity, the motion of a fluid is fully governed by the equilibrium of its pressure and inertia terms, which is also known as inertia flow. In the case of viscous fluid, it is assumed that in the initial stage of the flow, the motion of the flow is governed by inertia flow, but later as the effect of viscosity increases, the motion of the flow is instead, governed by the equilibrium of the pressure and viscosity terms. In this study, the terms "inertia region" and "viscous region" are also used to refer to a stage or regime where either the inertia or viscous flow dominates the motion of the fluid. The characteristic of inertia flow is investigated by modeling the dam break flow of inviscid fluid. From the analytical workout, it is noted that in inertia flow, the depth at the origin, h_m is inversely proportional to time $\left(t \propto t^{-1}\right)$, while the leading wave propagates proportionally with time $(L \propto t)$. Meanwhile, in the case of viscous fluid, the depth at the origin, h_m and leading wave, L are found to be proportional to time to the power of $-\frac{n}{3+2n}$ and $\frac{n}{3+2n}$ respectively, where n=1 for viscous Newtonian fluid, $n > 1$ or $n < 1$ for viscous non-Newtonian fluid. The analytical results describing the characteristics of the inertia region and viscous region of the flow are verified with 2 numerical models; a depth averaged model and MPS model. Numerical simulations with both models show good agreement with the analytical results. The verification of the existence of inertia and viscous regions and the findings on their characteristics through simple similarity assumptions in this study has provided an general insight of the flow characteristic of viscous fluid. In the sense of engineering application, this findings can be used to verify experimental or numerical results related of the determination of rheological properties of various industrial fluid. In industry field, the intrusion time of poisonous fluid and relatively dense gas can be estimated by knowing the characteristic of the flow in advance. This study also provide a stepping stone for future work to construct an integral model which can describe the motion of the flow immediately after the initiation of motion for the whole flow domain.

REFERENCES

1) Hosoda, T.,Kokada, T. and Miyagawa, T.: Study on a method of obtaining yield values of fresh concrete from slump flow test, *Concrete Lib. of JSCE* Vol.32, pp.29–41, 1998.
2) Shao, S. and Edmond Lo, Y.M.: Incompressible SPH method for simulating Newtonian and non-Newtonian flows with a free surface, *Adv. in Water Resource* Vol.26(7), pp.787–800(14), 2003.
3) Huppert, H.E.: The propagation of two dimensional and axisymmetric viscous gravity currents over a rigid horizontal surface, *J. Fluid. Mech.* Vol.121, pp.43–58, 1982.
4) Jain, S.C.: *Open Channel Flow,* John Wiley and Sons, Inc., New York, 2001.
5) Koshizuka, S.,Nobe, A. and Oka, Y.: Numerical analysis of breaking waves using the moving particle semi-implicit method, *Int. J. Num. Meth. Fluids.* Vol.26, pp.751–769, 1998.
6) Gotoh, H.,Ikari, H.,Memita, T. and Sakai, T.: Lagrangian particle method for simulation of wave overtopping on a vertical seawall, *Coastal. Eng. J.* Vol.47, Nos. 2 & 3, pp.157–181, 2005.
7) Ng, C. and Mei, C.C.: Roll waves on shallow layer of mud modeled as a power-law fluid, *J. Fluid. Mech.* Vol.263, pp.151–183, 1994.
8) Huang, X. and Garcia, M.H.: A Herschel-Bulkley model for mud flow down a slope, *J. Fluid. Mech.* Vol.374, pp.305–333, 1998.
9) Hogg, A.J. and Pritchard, D.: The effect of hydraulics resistance on dam-break and other shallow inertial flows, *J. Fluid. Mech.* Vol.501, pp.179–212, 2004.

(Received April 12, 2007)